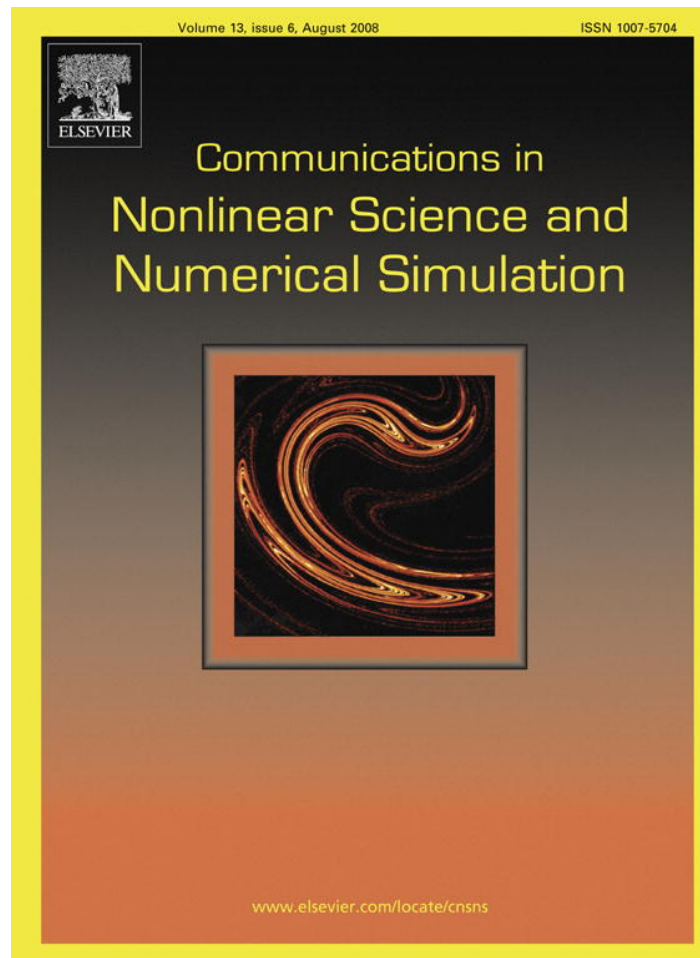


Provided for non-commercial research and education use.
Not for reproduction, distribution or commercial use.



This article was published in an Elsevier journal. The attached copy is furnished to the author for non-commercial research and education use, including for instruction at the author's institution, sharing with colleagues and providing to institution administration.

Other uses, including reproduction and distribution, or selling or licensing copies, or posting to personal, institutional or third party websites are prohibited.

In most cases authors are permitted to post their version of the article (e.g. in Word or Tex form) to their personal website or institutional repository. Authors requiring further information regarding Elsevier's archiving and manuscript policies are encouraged to visit:

<http://www.elsevier.com/copyright>



ELSEVIER

Available online at www.sciencedirect.com

 Communications in
 Nonlinear Science and
 Numerical Simulation

Communications in Nonlinear Science and Numerical Simulation 13 (2008) 1180–1193

www.elsevier.com/locate/cnsns

Phase-space growth rates, local Lyapunov spectra, and symmetry breaking for time-reversible dissipative oscillators

Wm.G. Hoover^{a,*}, Carol G. Hoover^a, Florian Grond^b

^a *HiTech Center, Great Basin College Elko, NV 89801, United States*

^b *Zentrum für Kunst und Medientechnologie, Lorenzstraße 19, D-76135 Karlsruhe, Germany*

Received 1 September 2006; received in revised form 27 October 2006; accepted 28 October 2006

Available online 8 December 2006

Abstract

We investigate and discuss the time-reversible nature of phase-space instabilities for several flows, $\dot{x} = f(x)$. The flows describe thermostated oscillator systems in from two through eight phase-space dimensions. We determine the local extremal phase-space growth rates, which bound the instantaneous comoving Lyapunov exponents. The extremal rates are point functions which vary continuously in phase space. The extremal rates can best be determined with a “singular-value decomposition” algorithm. In contrast to these precisely time-reversible local “point function” values, a time-reversibility analysis of the comoving Lyapunov spectra is more complex. The latter analysis is *nonlocal* and requires the additional storing and playback of relatively long (billion-step) trajectories.

All the oscillator models studied here show the *same* time reversibility symmetry linking their time-reversed and time-averaged “global” Lyapunov spectra. Averaged over a long-time-reversed trajectory, each of the long-time-averaged Lyapunov exponents simply changes signs. The negative/positive sign of the summed-up and long-time-averaged spectra in the forward/backward time directions is the microscopic analog of the Second Law of Thermodynamics. This sign changing of the individual global exponents contrasts with typical more-complex instantaneous “local” behavior, where there is no simple relation between the forward and backward exponents other than the local (instantaneous) dissipative constraint on their sum. As the extremal rates are point functions, they too always satisfy the sum rule.

© 2006 Elsevier B.V. All rights reserved.

PACS: 05.70.Ln; 05.45.–a; 05.45.Df; 02.70.Ns

Keywords: Lyapunov spectrum; Thermostats; Singular values; Fractals; Irreversibility

* Corresponding author. Tel.: +1 775 779 2266.

E-mail address: hooverwilliam@yahoo.com (Wm.G. Hoover).

1. Introduction

The *Lyapunov spectrum* of time-averaged phase-space growth and decay rates $\{\lambda_j = \langle \lambda_{jj}(t) \rangle\}$ is a promising long-standing tool for the understanding of both equilibrium and nonequilibrium phase-space flows. The individual exponents describe the mutually orthogonal one-dimensional growth rates, $\{\lambda_{jj}(t) = \dot{\delta}_j \cdot \delta_j / \delta_j^2\}$, at the surface of an infinitesimal phase-space hypersphere centered on, and comoving with, the phase-space trajectory. Our special interest here is time-reversible flows describing atomistic systems in nonequilibrium heat-conducting stationary states. Many interesting discoveries have already emerged from such studies [1–3]. Typical thermostated nonequilibrium systems have both a time-reversible dynamics and a formally reversible Lyapunov spectrum, with the exponents changing signs in the reversed flow. Despite this apparent simplicity the nonequilibrium systems typically generate dissipative multifractal strange attractors [4,5] and exhibit a “time’s arrow” “symmetry breaking”, with the sum over all exponents negative, rather than zero, indicating the exponentially fast collapse of phase volume \otimes onto a multifractal strange attractor [4,5],

$$\langle d \ln \otimes / dt \rangle = \sum_j \lambda_j < 0.$$

The formal reversibility of the instantaneous spectra is actually *incorrect*, as we illustrate in what follows.

Early work on the numerical determination of Lyapunov exponents involved the contributions of Stoddard and Ford [6], Benettin [7–9], and Shimada and Nagashima [10]. For simplicity we refer to the technique which developed from these three sets of workers as “Benettin’s” in what follows. Benettin used Gram–Schmidt orthonormalization [11] of a comoving set of phase-space basis vectors $\{\delta_i\}$, each associated with one of the Lyapunov exponents, to quantify Lyapunov instability. His approach characterizes attractors in terms of time averages of instantaneous values of the entire Lyapunov spectrum [7,9,10] of phase-space growth and decay rates. The individual time-dependent Lyapunov exponents can alternatively be expressed in terms of an upper-triangular matrix of continuous two-subscript Lagrange multipliers $\{\lambda_{i \leq j}(t)\}; \{\lambda_{i > j} \equiv 0\}$ [12–14]. The time-averaged [single-subscript] Lyapunov exponents are the time-averaged *diagonal* elements of the Lagrange-multiplier matrix which constrains the basis vectors—the j th offset vector has the N components:

$$\delta_j = \{\delta_{ij}\}; \quad 1 \leq i \leq N.$$

The N vectors in the N -dimensional phase space are constrained to remain orthonormal by the array of Lagrange multipliers $\{\lambda_{kj}\}$:

$$\begin{aligned} \dot{\delta}_{ij} = \sum_k [D_{ik} \delta_{kj} - \delta_{ik} \lambda_{kj}]; \quad \lambda_{k > j} \equiv 0; \quad \dot{x} = f(x); \quad D_{ij} \equiv \partial f_i / \partial x_j = \partial \dot{x}_i / \partial x_j; \quad \{\lambda_j\} \equiv \langle \lambda_{jj}(t) \rangle \\ \text{for } \left\{ \sum_k \delta_{ki} \delta_{kj} \equiv 0 \iff i \neq j; \quad \sum_k \delta_{ki} \delta_{ki} \equiv 1 \iff i = j \right\}. \end{aligned}$$

The dynamical matrix $D = \nabla_{\mathcal{X}} f$ describes the linearized flow which propagates the N offset vectors $\{\delta_j\}$. This continuous Lagrange multiplier approach is exactly equivalent to the small timestep limit of Benettin’s Gram–Schmidt procedure which we use in the present work.

Eckmann and Ruelle compiled a useful review of the early literature, published in 1985 [15], just before the subsequent flood of numerical results. The 20 productive years of numerical and analytical work since that review have led to a good qualitative understanding of phase-space structures far from equilibrium [4]. But there remain many unanswered questions concerning the symmetries and symmetry-breakings of the Lyapunov spectra for “time-reversible” systems. (The trajectory of a *time-reversible* system, played backward in time, satisfies exactly the same differential equations as does the forward trajectory. Hamilton’s mechanics is an example of this reversibility property.)

Typically the time-reversed motion in a dissipative system is even *less stable* than the forward-in-time evolution, and is hence unobservable [16]. Any numerical approximation to the reversed dynamics seeks out the attractor rather than following the repellor. This less-unstable attractor *obeys* the Second Law while the more-unstable repellor does not. Thus the numerical unobservability of the repellor is nicely in accord with Thermodynamics.

The numerical analysis of local trajectory instabilities for time-reversible nonequilibrium systems, as reflected in their instantaneous Lyapunov spectra, shows yet another, more detailed and intricate, instability. By recording and replaying the dissipative trajectory *backward* $[(q,p) \rightarrow (q,-p)$ or $dt \rightarrow -dt]$ and studying the sensitivity of this reversed motion to small perturbations $(\delta q, \delta p)$, the *reversed* comoving Lyapunov spectrum $\{\lambda_{\text{backward}}\}$ can be determined [17]. Formally, a reversed spectrum, with appropriate sign changes [as illustrated in Section 7] in the momentum-like [odd in the time] components of the offset vectors $\{\delta\}$, satisfies the set of instantaneous identities $\{+\lambda_{\text{forward}}(t) \equiv -\lambda_{\text{backward}}(t)\}$. Despite these formal identities, numerical work shows that there is generally no correlation between the forward and reversed instantaneous Lyapunov spectra $\{\lambda(t)\}$ [17–19]. In view of this additional missing symmetry it is desirable to check whether or not the long-time-averaged version of the symmetry relation remains valid:

$$\{\langle +\lambda_{\text{forward}} \rangle\} \stackrel{?}{=} \{\langle -\lambda_{\text{backward}} \rangle\}.$$

Here we study a series of generalizations of the simple harmonic oscillator problem, including not only the thermostat introduced by Nosé [20], but also some generalizations [21], and including also temperature *gradients* [22], as well as interoscillator coupling. The models we construct generate time-reversible but dissipative ($\langle \dot{\otimes} \rangle < 0$) phase-space structures, ranging from one-dimensional limit cycles to many-dimensional multifractal strange attractors. The consistent results coming from the present numerical analyses of these phase-space objects lend plausibility to the general behavior we infer for time-reversible systems far from equilibrium.

We begin by reviewing the geometric and thermodynamic significance of the Lyapunov Spectrum and by describing the Benettin algorithm for its determination. We then introduce a family of coupled thermostated harmonic oscillator problems, including a temperature gradient, which are well-suited to numerical analysis. We present precise numerical results for the forward and backward Lyapunov spectra for typical models, relating these to the bounding local extremal phase-space growth rates. The numerical work leads to two interesting conclusions. First, the global (time-averaged) Lyapunov spectrum simply changes sign in the time-reversed motion. Second, the local (instantaneous) Lyapunov spectrum has no such simple behavior. The second result, the lack of time-reversal symmetry of the individual instantaneous exponents, makes it essential to check the first. The failure of the Kaplan–Yorke conjecture (which is based on oversimplified geometric reasoning) underscores the need for numerical support of theoretical reasoning. The Kaplan–Yorke prediction of the information dimension [23], estimated from the Lyapunov spectrum, is poor [22] for some of these oscillator systems.

2. Computing the Lyapunov spectrum

The complete spectrum of Lyapunov exponents describes the N exponential rates of growth and decay in N -dimensional phase-space flows:

$$\dot{x} = f(x) \rightarrow \{\lambda(t)\} \rightarrow \{\lambda\} = \{\langle \lambda(t) \rangle\}.$$

Generally the instantaneous comoving rates $\{\lambda(t)\}$ are time-averaged. The averaging process requires following the progress of an infinitesimal basis set of orthogonal vectors, the offset vectors $\{\delta(t)\}$, with the set of N components. $\{\delta_{ij}\}; 1 \leq i \leq N$, composing the j th offset vector, centered on the flow trajectory $x(t)$ and associated with an array of Lagrange multipliers $\{\lambda_{kj}\}$:

$$\dot{\delta}_{ij} = \sum_k [D_{ik} \delta_{kj} - \delta_{ik} \lambda_{kj}(t)]; \quad \{\delta_j \rightarrow \lambda_j = \langle \lambda_{ij}(t) \rangle, t \rightarrow \infty\}.$$

The vectors can be thought of as describing the separation of a set of N “satellite” trajectories $\{x_j^{\text{sat}}\}$ constrained to rotate rigidly about the central “reference” trajectory x^{ref} :

$$\left\{ \delta_j = x_j^{\text{sat}} - x^{\text{ref}} \right\}.$$

A useful geometric picture visualizes the virtual infinitesimal distortion of a comoving “ball”, or hypersphere, of solutions centered on the reference trajectory. The distortion is virtual because the radius of the ball is actually kept constant, $|\delta_j| = \delta_0$, where δ_0 is a small (or even infinitesimal) constant length in the N -dimensional

phase space. The time-development of the comoving principal axes of the ball which *would* take place in the absence of the length constraints gives the Lyapunov spectrum. For the j th axis, the unconstrained equations of motion,

$$\dot{\delta}_{ij} = \dot{x}_{ij}^{\text{sat}} - \dot{x}_i^{\text{ref}}$$

are replaced by the constrained equations,

$$\dot{\delta}_{ij} = \dot{x}_{ij}^{\text{sat}} - \dot{x}_i^{\text{ref}} - \sum_k \delta_{ik} \lambda_{kj}; \quad \lambda_{k>j} \equiv 0,$$

which lead to the instantaneous spectra:

$$\left\{ \lambda_{jj}(t) = \frac{\delta_j \cdot D \cdot \delta_j}{\delta_j^2} \right\}.$$

Benettin developed a numerical algorithm equivalent to these analytic ideas in 1978 [7,9]. The algorithm imposes the orthogonality relations $\{(\delta_j \cdot \delta_k)_{j \neq k} = 0\}$ as well as the length constraints $\{(\delta_j \cdot \delta_j) = \delta_0^2\}$. Hoover and Posch [13] and Goldhirsch et al. [14] described and implemented the analytic continuous representation of Benettin's idea. They used an array of nonzero Lagrange Multipliers $\{\lambda_{k \leq j}\}$ to maintain the orthonormal relationship of the offset vectors [13,14] in the limit that the length of the offset vectors is infinitesimal.

The continuous algorithm generates automatically the set of Lagrange multipliers $\{\lambda_{jj}(t)\}$ which describe the Lyapunov spectrum as well as the offdiagonal multipliers $\{\lambda_{k < j}(t)\}$ which describe the relative rotation of the vectors. The N exponents describe the N growth/decay rates associated with the directions of the rotating vectors. Either finite (but small) [Benettin] or truly infinitesimal [Hoover and Posch] offset vectors can be used. For small N the accuracy and efficiency of the computation is improved by solving the *linearized* "tangent-space" equations for the evolution of the offset vectors:

$$D = \partial \dot{x} / \partial x.$$

For the linearized tangent-space system it is convenient to choose the vectors $\{\delta\}$ of unit length, $\{\delta_j^2 \equiv 1\}$.

The Lyapunov spectra for many nonequilibrium systems have been characterized. Time-reversible nonequilibrium motion equations typically lead to asymmetric Lyapunov spectra, with motion in the forward direction of time (which obeys the Second Law of Thermodynamics) less unstable than the reversed motion (which is unobservable and would violate the Second Law). The intimate connection of the Lyapunov spectrum (which describes changing phase volume) and thermodynamics follows from Gibbs' and Boltzmann's discovery that the logarithm of phase volume corresponds to thermodynamic entropy [4].

Mima et al. [24] recently studied the time-reversibility of a three-dimensional many-body stationary non-equilibrium heat flow. The geometry they chose was a periodic system with an aspect ratio of four ($L = 4W$). The system was composed of two Newtonian regions of width W separated by two thermostated reservoir regions, one hot and one cold, and also of width W : $(\dots N - H - N - C - N - H - N - C \dots)$. This geometry matches that of a two-dimensional system studied earlier [25]. Mima et al. were particularly interested in the time-reversibility properties, especially Lyapunov instability, of their conducting system. We consider this aspect of simpler time-reversible stationary heat flows here, following our earlier work [4,18,26,27] on the thermostated oscillators described in the following sections. The results of our investigation suggest that the time-averaged Lyapunov exponents simply change sign in the time-reversed flow, though the instantaneous exponents do not [18]. The observation that the overall phase-space flow shrinks, in the forward direction of time, but expands even more unstably in the reversed direction, is the microscopic equivalent of the Second Law of Thermodynamics. The systems investigated here are not only sufficiently complex to show this typical behavior, but are also sufficiently simple for precise numerical work.

In what follows we describe the harmonic oscillator model as well as its generalizations to temperature control, including a temperature gradient, with several interacting thermostated oscillators. We measure and discuss the time-reversibility of the Lyapunov spectra for these models. Our conclusions make up the final section.

3. Equilibrium harmonic oscillator

Consider first an equilibrium harmonic oscillator tracing out an elliptical constant-energy orbit in its (qp) phase space:

$$\mathcal{H} = \frac{1}{2}[(ps)^2 + (q/s)^2]; \quad \dot{\mathcal{H}} \equiv 0;$$

$$\dot{q} = +\partial\mathcal{H}/\partial p = +ps^{+2}; \quad \dot{p} = -\partial\mathcal{H}/\partial q = -qs^{-2}.$$

The dynamical matrix D , which describes the local phase-space deformation in the neighborhood of a (qp) phase point is

$$D = \begin{pmatrix} \partial\dot{q}/\partial q & \partial\dot{q}/\partial p \\ \partial\dot{p}/\partial q & \partial\dot{p}/\partial p \end{pmatrix} = \begin{pmatrix} 0 & +s^{+2} \\ -s^{-2} & 0 \end{pmatrix}; \quad \dot{\delta}q = +s^{+2}\delta p; \quad \dot{\delta}p = -s^{-2}\delta q.$$

The radial phase-space growth rate, in the direction given by the vector $(\delta q, \delta p)$ on an infinitesimal circle can be estimated by using a fixed very-small constant radius δ_0 , so that $\delta q^2 + \delta p^2 \equiv \delta_0^2$, is

$$\frac{\dot{\delta}q \cdot \delta q + \dot{\delta}p \cdot \delta p}{\delta q^2 + \delta p^2} = (s^{+2} - s^{-2})\delta q \delta p / \delta_0^2.$$

Evidently the *extremal* growth rates result from the choices $\delta p = \pm\delta q$:

$$\left(\frac{\dot{\delta} \cdot \delta}{\delta^2} \right)_{\max/\min} = \pm(s^{+2} - s^{-2})/2.$$

The oscillator's instantaneous Lyapunov exponents can be computed from the average values of the growth rates for the corresponding offset vectors. The results [28] are of course bounded by the extremal rates just calculated:

$$-(s^{+2} - s^{-2})/2 < \lambda_1(t), \lambda_2(t) < +(s^{+2} - s^{-2})/2; \quad \lambda_1 = \langle \lambda_1(t) \rangle = 0 = \langle \lambda_2(t) \rangle = \lambda_2;$$

$$\langle \lambda_1(t)^2 \rangle = \langle \lambda_2(t)^2 \rangle = (s^{+1} - s^{-1})^2/2.$$

It should be noted that a numerical algorithm for the extremal phase-space growth rates during a short time-step dt can most simply be obtained by “singular-value decomposition” [11,29]. The phase-space circle $\delta q^2 + \delta p^2 = \delta_0^2$ is propagated for a time interval dt by adding the unconstrained D matrix, times dt , to the unit matrix:

$$\delta(t + dt) = \begin{pmatrix} 1 & +s^{+2} dt \\ -s^{-2} dt & 1 \end{pmatrix} \times \delta(t).$$

Consider the example ($s = 2$; $dt = 0.001$). Singular value decomposition expresses the mapping of the offset vector from time t to time $t + dt$ as a product of three matrices, $U \times A \times V$, where the diagonal matrix A contains the “singular values” of the growth rate:

$$\begin{pmatrix} +1.00000 & +0.00400 \\ -0.00025 & +1.00000 \end{pmatrix} = \begin{pmatrix} +0.70636 & +0.70786 \\ -0.70786 & +0.70636 \end{pmatrix} \times \begin{pmatrix} +0.99813 & +0.00000 \\ +0.00000 & +1.00188 \end{pmatrix} \times \begin{pmatrix} +0.70786 & -0.70636 \\ +0.70636 & +0.70786 \end{pmatrix}.$$

For small dt the logarithms of the singular values, divided by dt , reproduce the extremal growth rates, $\pm(s^{+2} - s^{-2})/2 = \pm 1.875$:

$$(1/dt) \ln(0.99813) \simeq -1.875; \quad (1/dt) \ln(1.00188) \simeq +1.875.$$

The matrices U and V approximate the 45° rotation matrices associated with the axes of extremal growth, $\delta q = \pm\delta p$.

For symmetric matrices, singular value decomposition is *almost* equivalent to matrix eigenvalue-eigenvector analysis. The eigenvector matrices in the symmetric case are simply related, $U = V^t$, where the t indicates

transpose. Typical singular-value-decomposition software returns vectors of arbitrary sign, spoiling the relation which holds for eigenvectors, $U \times V = U \times U^t = I$. The phase-space growth rates of interest in statistical mechanics can be obtained from *symmetrized* matrices, either $(D + D^t)/2$ or $I + dt(D + D^t)/2$. Our very limited experiments with packaged software showed greater efficiency with the singular-value approach than with the standard eigenvalue approach.

4. Nosé–Hoover oscillator, at and away from equilibrium

The simplest form of the thermostated Nosé–Hoover harmonic oscillator equations [26] is

$$\ddot{q} = -q - \zeta \dot{q}; \quad \dot{\zeta} = \dot{q}^2 - T.$$

Though apparently locally dissipative and nonHamiltonian, Dettmann showed that there *is* a Hamiltonian giving rise to these motion equations:

$$\mathcal{H}_{\text{Dettmann}} = \left[\frac{p^2}{s} + sq^2 + s\zeta^2 + sT \ln s^2 \right] / 2 \equiv 0; \quad \zeta \equiv p_s;$$

$$\dot{q} = p/s; \quad \dot{p} = -qs; \quad \dot{s} = sp_s; \quad \dot{p}_s = \frac{p^2}{2s^2} - T - \frac{q^2 + \zeta^2 + T \ln s^2}{2} = \frac{p^2}{s^2} - T = \dot{q}^2 - T.$$

The Nosé–Hoover friction coefficient $\zeta = p_s$ is the momentum conjugate to Nosé’s “time-scaling” variable s :

$$\dot{s} = +\partial \mathcal{H} / \partial \zeta; \quad \dot{\zeta} = -\partial \mathcal{H} / \partial s.$$

For the history of Dettmann’s work see Ref. [30]. If we calculate the Lyapunov spectrum using Dettmann’s Hamiltonian we obtain four Lyapunov exponents satisfying the Hamiltonian symmetry requirements:

$$+\lambda_1 = -\lambda_4; \quad +\lambda_2 = -\lambda_3 \equiv 0,$$

which follow from the time-reversible nondissipative nature of Hamilton’s motion equations. In the case that $T = 1$ with a chaotic initial condition, such as

$$\{q_0, p_0, s_0, \zeta_0\} = \{q, p, s, \zeta\}_{t=0} = \{0, 5, 1, 0\},$$

we find the Lyapunov spectrum:

$$\{\lambda\} = \{+0.014, 0.000, 0.000, -0.014\}.$$

Compare this result to that obtained in a three-dimensional phase space from the Nosé–Hoover equations considered below.

The thermostating friction coefficient ζ , which maintains the oscillator temperature at $T \propto \dot{q}^2$, with a characteristic relaxation time τ , can be expressed in any one of three equivalent ways:

$$\dot{\zeta} = \frac{\dot{q}^2}{T} - 1 \quad \text{or} \quad \dot{\zeta} = [\dot{q}^2 - 1]/\tau^2 \quad \text{or} \quad \dot{\zeta} = \dot{q}^2 - T.$$

Even for a constant temperature T these simple equations for $(\ddot{q}, \dot{\zeta})$ have complex multifractal solutions in the three-dimensional phase $\{q, \dot{q} = p, \zeta\}$ space [26,27]. There are many interesting special cases, including not only chaotic solutions, but also stable regular solutions. Because the equilibrium Nosé–Hoover oscillator is a conventional Hamiltonian system its Lyapunov spectrum is symmetric, and sums to zero. Figs. 1 and 2 show the two typical solutions of the equilibrium equations for $T = 1$, one regular and one chaotic. The corresponding three-dimensional time-averaged Lyapunov spectra are as follows:

$$(q_0, p_0, \zeta_0) = (0, 1.55, 0) \rightarrow \{\lambda\} = \{0.000, 0.000, 0.000\};$$

$$(q_0, p_0, \zeta_0) = (0, 5.00, 0) \rightarrow \{\lambda\} = \{+0.014, 0.000, -0.014\};$$

Sprott analyzed this same chaotic case in Ref. [31, pp. 439–440], with the more precise results $\lambda_{1,3} = \pm 0.0138$. Notice that because the Nosé–Hoover three-dimensional dynamics just considered and the preceding four-dimensional Dettmann approach are exactly equivalent, the nonzero Lyapunov exponents for the two cases agree with one another.

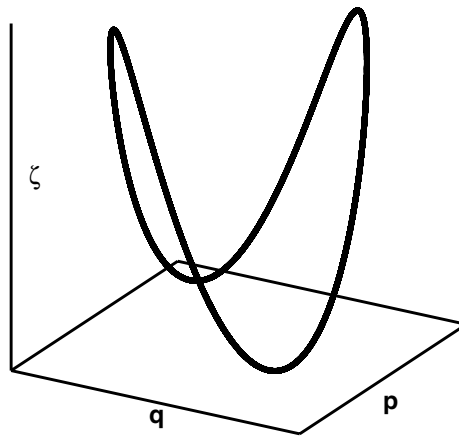


Fig. 1. Phase-space trajectory for the *regular* Nosé–Hoover oscillator, with initial conditions $(q, p, \zeta) = (0.00, 1.55, 0.00)$. The trajectory length shown here, 5.58, is a complete oscillator period. This calculation, like all others in the present work, uses fourth-order Runge–Kutta integration with a timestep $dt = 0.001$ [$-1.5 < q < +1.5$; $-2.0 < p < +2.0$; $-0.6 < \zeta < +0.6$].

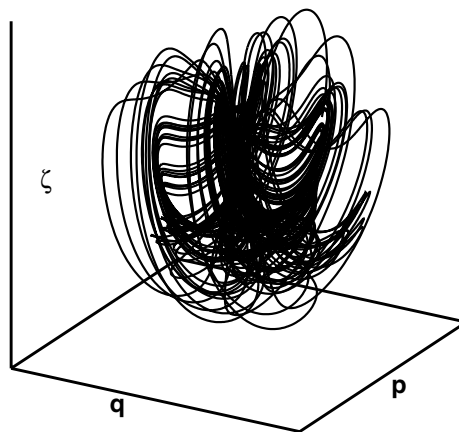


Fig. 2. Phase-space trajectory for the *chaotic* Nosé–Hoover oscillator, with initial conditions $(q, p, \zeta) = (0.00, 5.00, 0.00)$. The trajectory length shown here is 1000 [$-5 < q, p, \zeta < +5$].

The linearized phase-space growth rate in the direction $(\delta q, \delta p, \delta \zeta)$ at the phase-space location $(q + \delta q, p + \delta p, \zeta + \delta \zeta)$ for the equilibrium Nosé–Hoover oscillator follows from the dynamical matrix derivatives:

$$\delta q \cdot \dot{\delta q} + \delta p \cdot \dot{\delta p} + \delta \zeta \cdot \dot{\delta \zeta} = -\zeta \delta p^2 + p \delta p \delta \zeta.$$

The extremal rates follow from the plane-polar-coordinate relations in the $(\delta p, \delta \zeta)$ plane:

$$\begin{aligned} \delta p &\equiv \sin(\theta); & \delta \zeta &\equiv \cos(\theta); & \frac{d}{d\theta} [-\zeta \delta p^2 + p \delta p \delta \zeta] &= 0 \\ &\rightarrow \tan(2\theta) &= (p/\zeta). \end{aligned}$$

In Figs. 3 and 4 we show the extremal growth rates and the instantaneous Lyapunov spectra, for the regular and chaotic orbits of Figs. 1 and 2. In the general case the extremal growth rates could be obtained in any one of three ways: (i) Monte Carlo sampling of rates in tangent-space, with a decreasing jump length; (ii) a “simplex” method [11], in which a number of sampling points just exceeding the dimensionality of the space is used to add a “better” point to the sample while discarding the “worst” point, and (iii) singular-value decomposition of the propagator matrix. Combined with Gram–Schmidt orthonormalization these techniques lead to a local growth-rate spectrum analogous to the Lyapunov spectrum. Unlike the Lyapunov spectrum the growth-

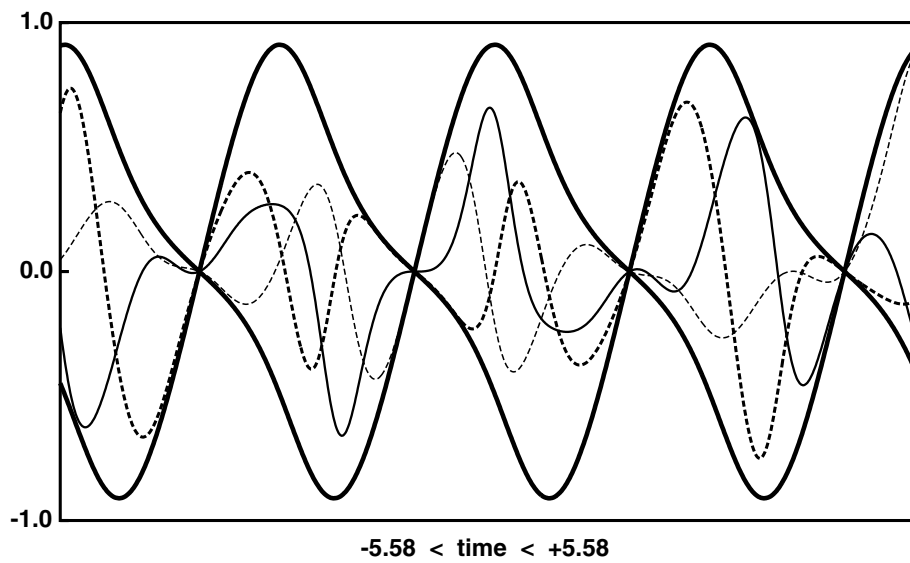


Fig. 3. Local Lyapunov exponents and extremal growth rates (heavy lines) for a typical two-period segment of the regular Nosé–Hoover oscillator trajectory of Fig. 1. The extremal lines do not cross. The time-averaged Lyapunov exponents all vanish. The interior heavy and light dashed lines show $\lambda_1(t)$ and $\lambda_3(t)$. The light interior solid line is $\lambda_2(t)$.

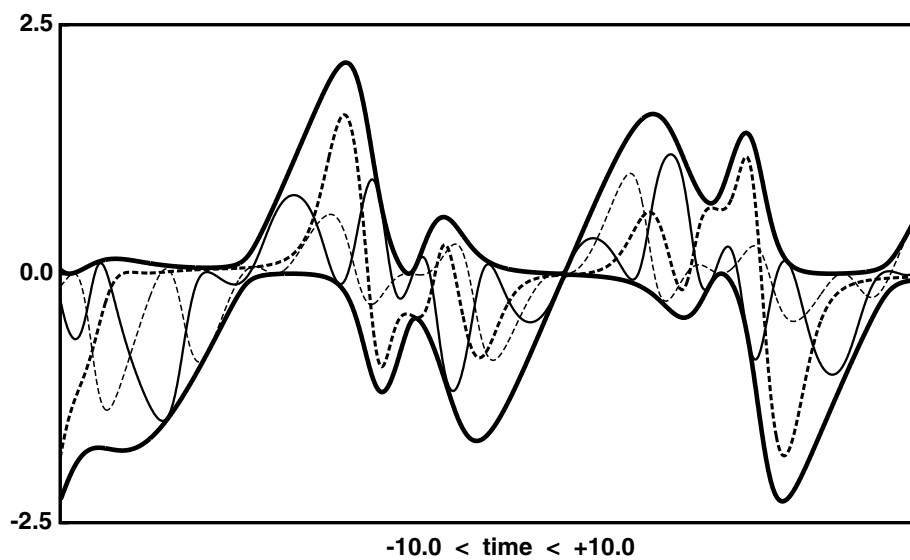


Fig. 4. Local Lyapunov exponents and extremal growth rates (heavy lines) for a typical segment of length 20 from the chaotic Nosé–Hoover oscillator trajectory of Fig. 2. The interior heavy and light dashed lines show $\lambda_1(t)$ and $\lambda_3(t)$. The light interior solid line is $\lambda_2(t)$. The long-time-averaged Lyapunov exponents are $(+0.014, 0.000, -0.014)$.

rate spectrum is local and independent of the direction of time even in the nonequilibrium case. For some reason the computation of these local growth rates is seldom, if at all, done or discussed. The extremal rates are typically orders of magnitude bigger than the *time-averaged* Lyapunov exponents for the systems studied here.

Consider a *nonequilibrium* case [18] where the temperature depends strongly on the coordinate q of a heat-conducting oscillator,

$$0 < T(q) \equiv T_q = 1 + \tanh(q) < 2.$$

The motion is dissipative, with overall heat transfer from larger values of q and T to smaller values. It might be thought odd to define temperature for a system with only a single degree of freedom, such as the nonequilib-

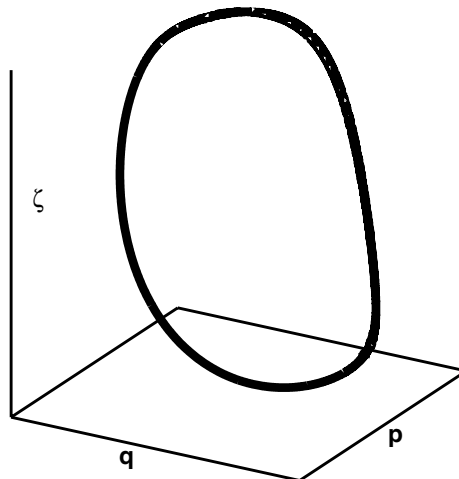


Fig. 5. Phase-space limit-cycle trajectory for the *nonequilibrium* Nosé–Hoover oscillator, with temperature $T = 1 + \tanh(q)$. The period for this limit cycle is 13.75 $[-3 < q < +1; -4 < p < +1; -4 < \zeta < +4]$.

rium oscillator. This idea is really not at all strange, and is fully consistent with Gibbs’ equilibrium canonical-ensemble result that *every* Cartesian degree of freedom satisfies the long-time-averaged relationship:

$$kT_{\text{ensemble}} \equiv \langle p^2/m \rangle.$$

Here, in the single-thermostated-oscillator case, the motion in (q, \dot{q}, ζ) space quickly reaches a one-dimensional limit cycle:

$$\ddot{q} = -q - \zeta \dot{q}; \quad \dot{\zeta} = \dot{q}^2 - [1 + \tanh(q)] \rightarrow \{\lambda\} = \{0.0000, -0.1095, -1.2155\}.$$

The two minus signs describe the time-averaged phase-space shrinkage toward a stable periodic attracting orbit. Fig. 5 shows the limit cycle, which has a period of 13.75. Fig. 6 shows that not only are the extremal growth rates periodic; the associated instantaneous Lyapunov exponents are periodic too.

The orbit can be stored, and run backwards, either replaying the stored values of $\{q, \dot{q}, \zeta\}$ unchanged:

$$dt \rightarrow -dt; \quad \ddot{q} = +q + \zeta \dot{q}; \quad \dot{\zeta} = -\dot{q}^2 + [1 + \tanh(q)],$$

or, with $\{Q, P, Z\} = \{q, -p, -\zeta\}$,

$$dt \rightarrow dt; \quad \ddot{Q} = -Q - Z \dot{Q}; \quad \dot{Z} = \dot{Q}^2 - [1 + \tanh(Q)].$$

Either of these equivalent interpretations of reversibility provides the same *unstable* Lyapunov spectrum, accurate to four significant figures:

$$\{\lambda\} = \{+1.2155, +0.1095, 0.0000\}.$$

The reversal does *not* hold for the instantaneous exponents $\lambda(t)$. Fig. 6 shows the exponents (along with the maximum and minimum growth rates) both forward and backward in time. Though both evolutions are periodic and trace out the same phase-space trajectories, there is no simple relation linking the individual instantaneous forward and backward exponents. We next consider more-complex systems, still time-reversible, and also chaotic, with at least one positive Lyapunov exponent, but still *dissipative*, with a negative time-averaged exponent sum.

5. Doubly-thermostated conducting oscillator

The second moment $\langle p^2 \rangle$ of the Nosé–Hoover oscillator is controlled by the friction coefficient ζ . Adding a *second* control variable ξ , controlling in addition the *fourth* moment [18,21,22,32] $\langle p^4 \rangle$, provides not only an ergodic solution for the equilibrium oscillator but also a more complicated set of nonequilibrium systems within the four-dimensional (q, p, ζ, ξ) phase space:

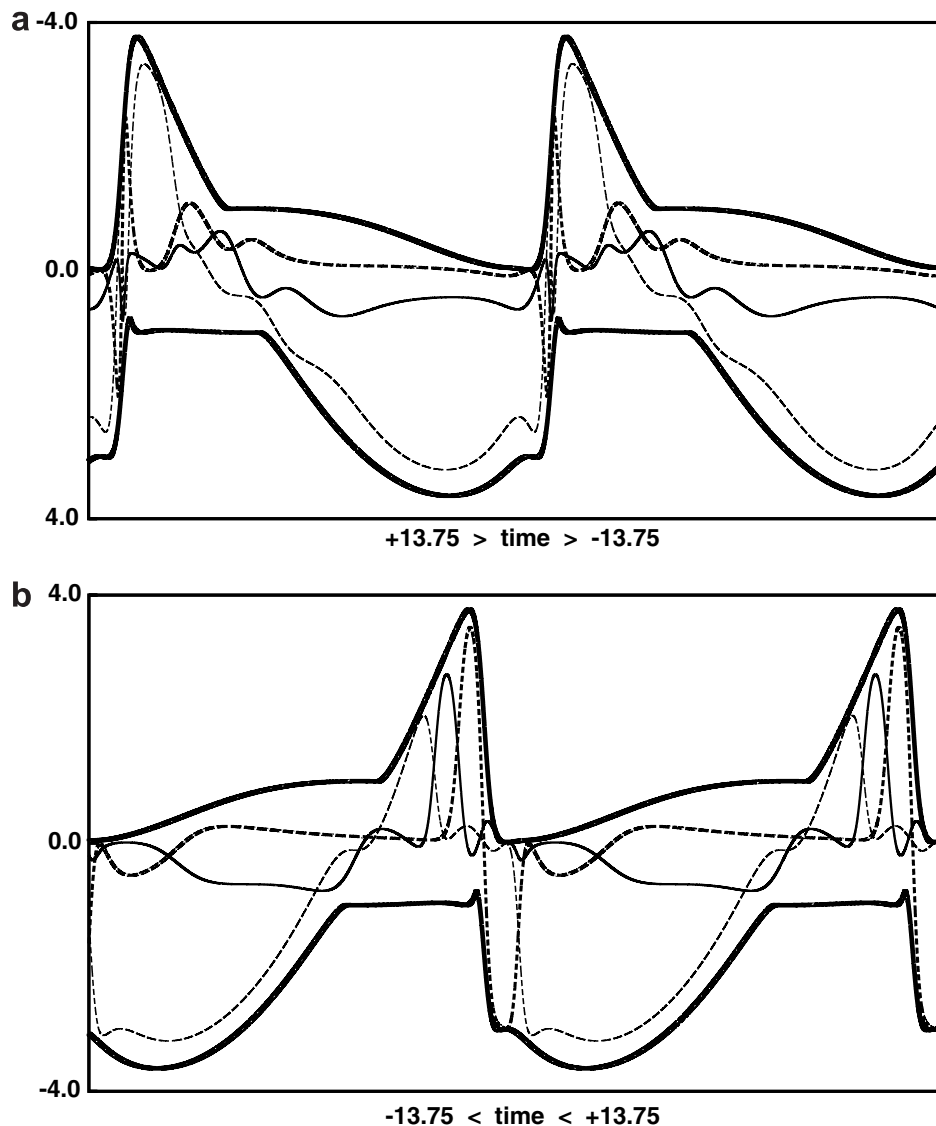


Fig. 6. Local Lyapunov exponents and extremal growth rates (heavy lines) for two periods of the nonequilibrium limit cycle shown in Fig. 5. Results in both the reversed (shown at the top) and forward (shown below) directions of time are shown. The interior heavy and light dashed lines show $\lambda_1(t)$ and $\lambda_3(t)$. The light interior solid line is $\lambda_2(t)$. Note the lack of correspondence between the forward and backward instantaneous Lyapunov exponents.

$$\dot{q} = p; \quad \dot{p} = -q - \zeta p - \xi p^3; \quad \dot{\zeta} = p^2 - T_q; \quad \dot{\xi} = p^4 - 3p^2 T_q; \quad T_q = 1 + \epsilon \tanh(q).$$

At equilibrium, with $\epsilon = 0$ and $T = 1$, the Lyapunov spectrum for the doubly-thermostated oscillator exhibits the expected symmetry:

$$\{\lambda\} = \{+0.066, 0.000, 0.000, -0.066\}.$$

A nonequilibrium oscillator system can be constructed by choosing a coordinate-dependent temperature T_q , so that the oscillator is exposed to a temperature gradient. For the strongly *nonequilibrium* choice $\epsilon = 1 \rightarrow T_q = 1 + \tanh(q)$ the solution generates an ergodic strange attractor with an information dimension (based on the four-dimensional phase-space averaged bin sums $\langle f \ln f \rangle$) of $D_{\text{info}} = 2.56$ and a Lyapunov spectrum with *broken symmetry*:

$$\{\lambda\} = \{+0.073, +0.000, -0.091, -0.411\}.$$

Fig. 7 shows the (qp) and $(\zeta\xi)$ projections of the strange attractor into two two-dimensional subspaces. The predicted Kaplan–Yorke dimension from this spectrum is $D_{\text{KY}} = 2 + \frac{73}{91} \approx 2.80$. Ordinarily the Kaplan–Yorke

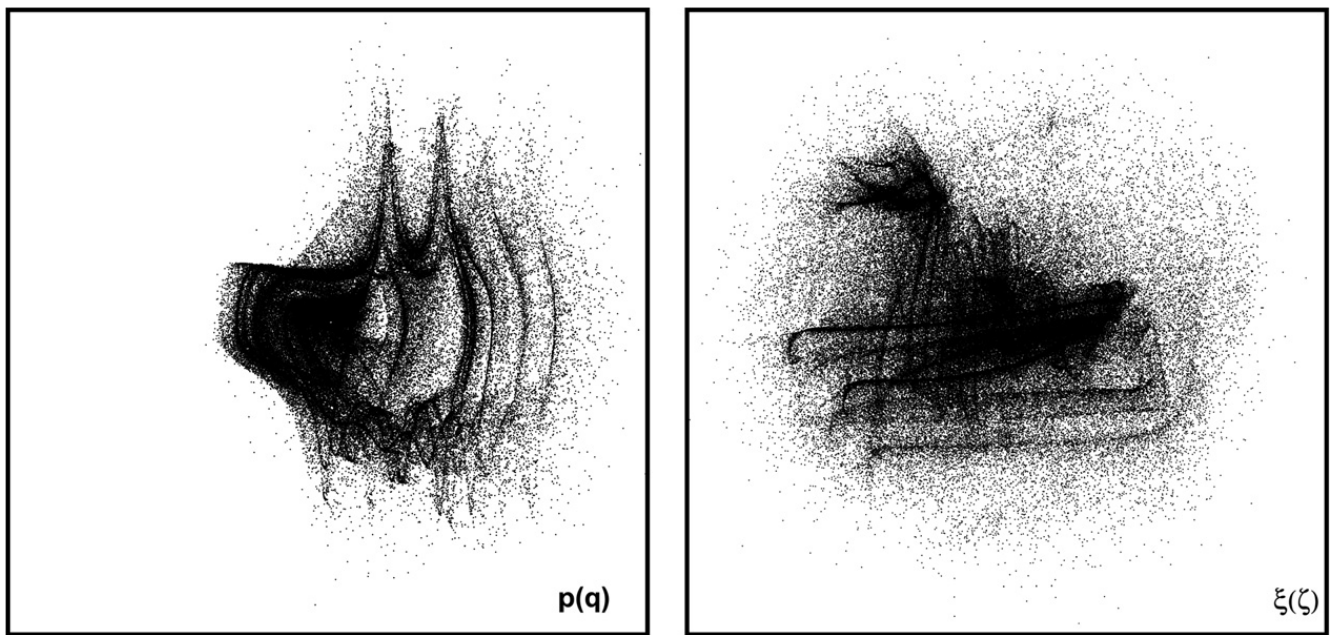


Fig. 7. Phase-space projected distributions for the chaotic nonequilibrium (q, p, ζ, ξ) oscillator, with $T = 1 + \tanh(q)$. 200,000 points, separated by $1000dt$, are shown $[-6 < q, p, \zeta, \xi < +6]$.

dimension is thought to provide a good estimate for the information dimension. The definite failure of the estimate here reflects the rapid rotation of the offset vectors, without which rotation the relation would be exact. On physical grounds the Kaplan–Yorke dimensionality error cannot exceed unity.

The instantaneous behavior of the Lyapunov exponents, together with that of their bounds from singular-value decomposition, is both complicated and sporadic. Fig. 8 illustrates the time-dependence of the upper and lower bounds for a short but typical segment of this chaotic trajectory. This phase-space flow, in only four dimensions, already illustrates two typical aspects of many-body flows. There are huge fluctuations in the exponents with wide disparities between the local (instantaneous) Lyapunov and their global (long-time-averaged) values. Like the bounds shown here, the local exponents reach values two orders of magnitude greater

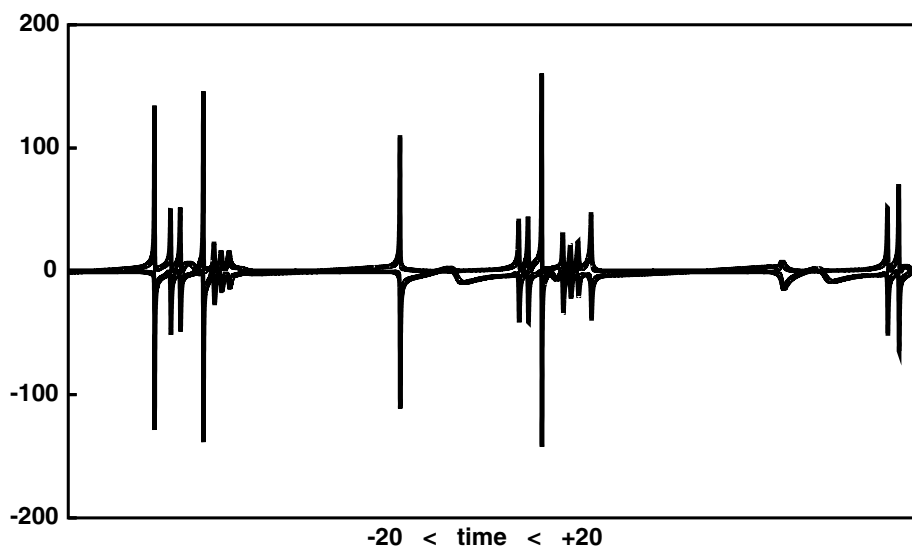


Fig. 8. Extremal instantaneous growth rates (from singular-value decomposition) for a segment of the chaotic (q, p, ζ, ξ) trajectory of Fig. 7. Rates in the reversed directions of time simply change sign.

than their averages. Just as in the simpler Nosé–Hoover case there is no special relationship between the instantaneous forward and backward exponents.

Grond and his coworkers investigated an alternative instantaneous “Wolf-algorithm” definition of local Lyapunov exponents [33,34], in which the direction of one offset vector is constrained to be parallel to the phase-space trajectory. In this case the local exponents measure the surface growth rates of an infinitesimal hypercylinder paralleling the trajectory. This approach leads to a slight reduction in the fluctuations of the local exponents. We found that the long-time-averaged exponents—using Wolf’s modification of Benettin’s original idea—lead to no detectable changes in the long-time-averaged Lyapunov spectrum.

The transformation of the phase-space distribution, from a smooth Gibbsian distribution to a *fractal* distribution, is in fact *typical* of nonequilibrium systems treated with Nosé–Hoover mechanics [4]. Let us consider next a two-body example, before discussing the more general situation, together with its implications for non-equilibrium statistical mechanics.

6. Coupled doubly-thermostated harmonic oscillators

A many-body thermostated oscillator system can be developed by coupling the oscillator coordinates. As an example, consider the addition of pairwise-additive forces from the coupling potential,

$$\phi_{12} = \frac{\kappa}{2}(q_1 - q_2)^2 \equiv \frac{1}{2}(q_1 - q_2)^2$$

to the thermostated-oscillator equations of motion for two oscillators. In the *nonequilibrium* case, where the control variables for the two oscillators react to the individual temperatures,

$$T_1 = 1 + \tanh(q_1) \rightarrow (\dot{\zeta}_1, \dot{\xi}_1); \quad T_2 = 1 + \tanh(q_2) \rightarrow (\dot{\zeta}_2, \dot{\xi}_2),$$

the forward and reversed Lyapunov spectra in the eight-dimensional phase space turn out be simply related:

$$\{\lambda\}_{f/b} = \{\pm 0.231, \pm 0.105, \pm 0.025, 0.000, \mp 0.045, \mp 0.129, \mp 0.262, \mp 0.463\}.$$

The upper signs correspond to the usual dynamics. The lower signs were obtained by playing the eight-dimensional phase-space trajectory backward, analyzing the replayed trajectory for the long-time-averaged spectrum. To the numerical accuracy of the calculation, (± 0.001) the time-averaged spectrum reverses sign perfectly. For the nonequilibrium system evolving forward in time the Kaplan–Yorke dimension is 6.71 in the eight-dimensional phase space.

7. Formal [incorrect!] Lyapunov-spectrum reversibility

In general, time-reversible equations of motion imply (formally, but *incorrectly*) that the *instantaneous* Lyapunov exponents all change sign in a time-reversed motion. It seems simplest to illustrate this not-so-well-known fact by detailing a sufficiently-complicated example to make the general result plausible. Accordingly, consider the full equations of motion, in three-dimensional phase space, for a Nosé–Hoover oscillator with unit mass, temperature, and relaxation time,

$$\dot{q} = p; \quad \dot{p} = -q - \zeta p; \quad \dot{\zeta} = p^2 - 1.$$

A time-reversed trajectory portion satisfies the same equations of motion, provided that the initial conditions in the reversed portion are properly chosen. If, at the end of the forward-in-time portion the signs of p and ζ are changed, the backward-in-time trajectory is related to its forward-in-time twin as follows:

$$\{\dot{q}, \dot{p}, \dot{\zeta}, q, p, \zeta\}_{\text{backward}} = \{-\dot{q}, +\dot{p}, +\dot{\zeta}, +q, -p, -\zeta\}_{\text{forward}}.$$

Notice that both sides of the \dot{q} equation change sign in the reversed motion while the \dot{p} and $\dot{\zeta}$ equations are unchanged in sign.

The formal time-reversibility of the Lyapunov exponents is only slightly more complicated to see. In the three-dimensional $\{q, p, \zeta\}$ phase space each of the three orthogonal offset vectors has three components. Here

are the full motion equations for the three three-dimensional infinitesimal offset vectors, forward in time, for this example:

$$\begin{aligned} \dot{\delta}_{q1} &= +\delta_{p1} - \delta_{q1}\lambda_{11}; & \dot{\delta}_{p1} &= -\delta_{q1} - \zeta\delta_{p1} - p\delta_{\zeta1} - \delta_{p1}\lambda_{11}; & \dot{\delta}_{\zeta1} &= +2p\delta_{p1} - \delta_{\zeta1}\lambda_{11}. \\ \dot{\delta}_{q2} &= +\delta_{p2} - \delta_{q2}\lambda_{22} - \delta_{q1}\lambda_{12}; & \dot{\delta}_{p2} &= -\delta_{q2} - \zeta\delta_{p2} - p\delta_{\zeta2} - \delta_{p2}\lambda_{22} - \delta_{p1}\lambda_{12}; & \dot{\delta}_{\zeta2} &= +2p\delta_{p2} - \delta_{\zeta2}\lambda_{22} - \delta_{\zeta1}\lambda_{12}. \\ \dot{\delta}_{q3} &= +\delta_{p3} - \delta_{q3}\lambda_{33} - \delta_{q2}\lambda_{23} - \delta_{q1}\lambda_{13}; & \dot{\delta}_{p3} &= -\delta_{q3} - \zeta\delta_{p3} - p\delta_{\zeta3} - \delta_{p3}\lambda_{33} - \delta_{p2}\lambda_{23} - \delta_{p1}\lambda_{13}; \\ \dot{\delta}_{\zeta3} &= +2p\delta_{p3} - \delta_{\zeta3}\lambda_{33} - \delta_{\zeta2}\lambda_{23} - \delta_{\zeta1}\lambda_{13}. \end{aligned}$$

Notice that by allowing all of the various $\{\delta_{pj}, \delta_{\zeta j}, \lambda_{kj}\}$ to change sign in the reversed Lyapunov analysis [along with $(p(t), \zeta(t))$ on the reference trajectory itself] that both sides of the three equations for $\{\dot{\delta}_{qj}\}$ change sign while both sides of the remaining six equations, for $\{\dot{\delta}_{pj}, \dot{\delta}_{\zeta j}\}$, do not. Thus the time reversibility guarantees that any trajectory analysis proceeding forward in time corresponds to a twin trajectory proceeding backward in time [and satisfying the same 12 differential equations] with the *instantaneous* Lyapunov spectrum reversed:

$$\{+\lambda_{kj}\}_{\text{forward}} \equiv \{-\lambda_{kj}\}_{\text{backward}}.$$

8. Conclusions for the general situation

Generally, thermostated Nosé–Hoover mechanics makes it possible to connect the time-rates-of-change of phase volume \otimes , the phase-space probability density f , and the external entropy-production rate \dot{S} to the second-moment friction coefficients $\{\zeta_i(T_i)\}$ and to the time-averaged Lyapunov spectrum $\{\lambda_i \equiv \langle \lambda_i(t) \rangle\}$, where as usual the angular brackets indicate a *long* time average:

$$-\langle d \ln \otimes / dt \rangle \equiv +\langle d \ln f / dt \rangle \equiv \sum_i \langle \zeta_i \rangle \equiv \langle \dot{S} / k \rangle \equiv -\sum_j \langle \lambda_j(t) \rangle = -\sum_j \lambda_j \geq 0.$$

The final inequality is the Second Law of Thermodynamics. The chain of inequalities, which follow exactly from the Nosé–Hoover equations of motion, relate the loss of microscopic phase-space volume \otimes (and dimensionality) to the macroscopic rate of entropy production.

The fractal nature of the nonequilibrium distributions, together with the time-reversibility of the motion equations, also provides a physical interpretation of irreversibility [4,5,16]. Motion in the forward direction is invariably less unstable than motion in the reverse direction;

$$\lambda_{\text{forward}} \equiv -\lambda_{\text{backward}} \rightarrow \left[\sum_{\text{forward}} \lambda_j < 0; \otimes \rightarrow 0 \right] \leftrightarrow \left[\sum_{\text{backward}} \lambda_j > 0; \otimes \rightarrow \infty \right].$$

Thus *any* uncertainty or perturbation to a trajectory, no matter how small, will, when the trajectory is reversed, cause the trajectory to fail to reverse precisely. Instead, the unstable dynamics will choose the direction of increasing entropy with overwhelming probability. Repellor trajectories can be generated only by replaying stored trajectories backward.

If the distortion of an infinitesimal phase-space hyperball could be stably reversed then it would be an “obvious” consequence that the Lyapunov spectrum changes sign in the reversed motion. The fact that the instantaneous offset vectors $\{\delta(t)\}$ do not simply reverse made the change of sign of the time-averaged Lyapunov exponents a matter for the investigation we carried out here. The failure of the Kaplan–Yorke conjecture for these systems underscores the need for careful checks of intuitive reasoning. We found that a variety of systems *do* satisfy the time-averaged sign-change identity. A proof of this result, or even a strong plausibility argument for it, would be very welcome.

The exact connection linking singular-value decomposition to phase-space growth rates provides an efficient bound on the instantaneous Lyapunov exponents. The fluctuations in the exponents are so large that the singular value bounds are not particularly useful estimates for the exponents and cannot even be used to predict the presence or absence of chaos. The extremal values from singular-value decomposition do have

an intrinsic interest of their own—they are certainly simpler than the Lyapunov exponents. As point functions they also have the exact time-antisymmetry which the nonequilibrium Lyapunov spectrum lacks.

Acknowledgements

A portion of this work was carried out at the HiTech Center, Great Basin College (Elko, Nevada) with the support of the Academy of Applied Science (Concord, New Hampshire) through the 2006 Research and Engineering Apprenticeship Program. We appreciate the comments and suggestions made by Harald Posch (Vienna University), Stefano Ruffo (Florence), Oyeon Kum (Pohang University, Korea), Giancarlo Benettin (Padua), and Clint Sprott (University of Wisconsin). This work was stimulated by conversations with Hiroyuki Hyuga and Toshiki Mima at the Symposium on Progress and Future Prospects in Molecular Dynamics Simulation in Memory of Professor Shuichi Nosé (Keio University, Yokohama, 6–8 June 2006). We wish to dedicate this work to the memory of Professor Nosé.

References

- [1] Dettmann CP, Morriss GP. *Phys Rev E* 1996;53:R5545.
- [2] Hoover WmG, Boercker K, Posch HA. *Phys Rev E* 1998;57:3911.
- [3] Hoover WmG, Posch HA, Aoki K, Kusnezov D. *Euro Lett* 2002;60:337.
- [4] Hoover WmG. Time reversibility, computer simulation, and chaos. Singapore: World Scientific; 1999, 2001.
- [5] Holian BL, Hoover WG, Posch HA. *Phys Rev Lett* 1987;59:10.
- [6] Stoddard SD, Ford J. *Phys Rev A* 1973;8:1504.
- [7] Benettin G, Galgani L, Giorgilli A, Strelcyn JM. *Meccanica* 1980;15:9.
- [8] Benettin G, Galgani L, Strelcyn JM. *Phys Rev A* 1976;14:2338.
- [9] Benettin G, Galgani L, Giorgilli A, Strelcyn JM. *Compt Rend* 1978;286A:431.
- [10] Shimada I, Nagashima T. *Prog Theor Phys* 1979;61:1605.
- [11] Press WH, Flannery BP, Teukolsky SA, Vetterling WT. *Numerical recipes, the art of scientific computing*. London: Cambridge University Press; 1986.
- [12] Posch HA, Hoover WG. *Phys Rev A* 1989;39:2175.
- [13] Hoover WG, Posch HA. *Phys Lett A* 1987;123:227.
- [14] Goldhirsch I, Sulem PL, Orszag SA. *Physica D* 1987;27:311.
- [15] Eckmann JP, Ruelle D. *Rev Mod Phys* 1985;57:617.
- [16] Moran B, Hoover WG, Bestiale S. *J Stat Phys* 1987;48:709.
- [17] Hoover WG, Tull (now Hoover CG) CG, Posch HA. *Phys Lett A* 1988;131:211.
- [18] Hoover WmG, Hoover CG, Posch HA. *Comp Meth Sci Tech* 2001;7:55.
- [19] Legras B, Vautard R. *Pred* 1996;1:135.
- [20] Nosé S. *Prog Theor Phys Suppl* 1991;103:1.
- [21] Hoover WmG, Holian BL. *Phys Lett A* 1996;211:253.
- [22] Hoover WmG, Hoover CG, Posch HA, Codelli JA. *CNSNS* 2007;12:214.
- [23] Kaplan JL, Yorke JA. *Proceedings of the functional differential equations and approximations of fixed points*. Berlin: Springer-Verlag; 1979. p. 204.
- [24] Mima T, Yasuoka K, Nosé S. Abs P-49, Symposium on progress and future prospects in molecular dynamics simulation in memory of Professor Shuichi Nosé, Keio University, Yokohama, 2007.
- [25] Hoover WmG, Posch HA. *Phys Rev E* 1996;54:5142.
- [26] Posch HA, Hoover WG, Vesely FJ. *Phys Rev A* 1986;33:4253.
- [27] Hoover WmG, Hoover CG, Isbister DJ. *Phys Rev E* 2001;63:026209.
- [28] Hoover WG, Hoover CG, Posch HA. *Phys Rev A* 1990;41:2999.
- [29] Stewart G. *SIAM Rev* 1993;35:551.
- [30] Hoover WG. *Physica A* 1997;240:1.
- [31] Sprott JC. *Chaos and time-series analysis*, Oxford UP, 2003, 2004.
- [32] Hoover WG, Aoki K, Hoover CG, DeGroot SV. *Physica D* 2004;187:253.
- [33] Grond F, Diebner HH, Sahle S, Mathias A, Fischer S, Rössler OE. *Chaos Solitons Fract* 2003;16:841.
- [34] Grond F, Diebner HH. *Chaos Solitons Fract* 2005;23:1809.